

Crystal Structures of α -Mercaptoacyldipeptides in the Thermolysin Active Site: Structural Parameters for a Zn Monodentation or Bidentation in Metalloendopeptidases[‡]

J. F. Gaucher,[§] M. Selkti,[§] G. Tiraboschi,^{||} T. Prangé,^{§,⊥} B. P. Roques,^{*,||} A. Tomas,[§] and M. C. Fournié-Zaluski^{||}

Laboratoire de Cristallographie & RMN Biologiques, CNRS EP 2075, UFR des Sciences Pharmaceutiques et Biologiques, 4 Avenue de l'Observatoire, 75270 Paris Cedex 06, France, and Département de Pharmacochimie Moléculaire & Structurale, INSERM U266, CNRS UMR 8600, UFR des Sciences Pharmaceutiques et Biologiques, 4 Avenue de l'Observatoire, 75270 Paris Cedex 06, France

Received May 7, 1999; Revised Manuscript Received July 20, 1999

ABSTRACT: Three α -mercaptoacyldipeptides differing essentially in the size of their C-terminal residues have been crystallized in the thermolysin active site. A new mode of binding was observed for **3** [HS-CH(CH₂Ph)CO-Phe-Tyr] and **4** [HS-CH((CH₂)₄CH₃)CO-Phe-Ala], in which the mercaptoacyl moieties act as bidentates with Zn–S and Zn–O distances of 2.3 and 2.4 Å, respectively, the side chains fitting the S₁, S₁', and S₂' pockets. Moreover, a distance of 3.1 Å between the sulfur atom and the OE1 of Glu¹⁴³ suggests that they are H-bonded and that one of these atoms is protonated. This H-bond network involving Glu¹⁴³, the mercaptoacyl group of the inhibitor, and the Zn ion could be considered a “modified” transition state mimic of the peptide bond hydrolysis. Due to the presence of the hindering (5-phenyl)proline, the inhibitor HS-CH(CH₂Ph)CO-Gly-(5-Ph)Pro (**2**) interacts through the usual Zn monodentation via the thiol group and occupancy of S₁' and S₂' subsites by the aromatic moieties, the proline ring being outside the active site. The inhibitory potencies are consistent with these structural data, with higher affinities for **3** (4.2×10^{-8} M) and **4** (4.8×10^{-8} M) than for **2** (1.2×10^{-6} M). The extension of the results, obtained with thermolysin being considered as the model of physiological zinc metallopeptidases, allows inhibitor-recognition modes for other peptidases, such as angiotensin converting enzyme and neutral endopeptidase, to be proposed and opens interesting possibilities for the design of new classes of inhibitors.

Thermolysin (TLN,¹ EC 3.4.24.4) is a proteolytic enzyme with a molecular weight of 34 600 isolated from *Bacillus thermoproteolyticus*. This enzyme contains one zinc ion that is essential for hydrolytic activity and four calcium ions that are required for its thermostability. Crystallographic studies with thermolysin complexed with a variety of inhibitors have provided evidence for the mode of interaction of extended substrates with the S₂–S₂'² subsites of the enzyme (*1*) and have suggested a mechanism of action for peptide hydrolysis (*2, 3*).

Physiological enzymes such as neutral endopeptidase (neprilysin, NEP, EC 3.4.24.11) (reviewed in ref 4), angiotensin converting enzyme (ACE, EC 3.4.15.1) (reviewed in ref 5), and endothelin converting enzyme (reviewed in ref 6) belong to the same family of metallopeptidases as TLN. All these enzymes possess the two consensus sequences HexxH and ExxxD (*7*), located in helical structures, which constitute the catalytic domain of TLN (*2*). These analogies have been supported by results of mutagenesis experiments carried out either with NEP alone or in parallel with both NEP and TLN (*8, 9*), allowing a three-dimensional model of the active site of NEP derived from that of TLN to be proposed (*10*). Therefore, crystallographic data for various thermolysin–inhibitor complexes are useful both in understanding the mechanism of action of these enzymes and in designing potent inhibitors (*11, 12*).

Thus, TLN is now classically used as a three-dimensional model to identify the interactions stabilizing an inhibitor in the active site of NEP (*10*) or to design new NEP inhibitors (*4, 13, 41*). On the basis of these results, we have proposed that α -mercaptoacyldipeptides such as (2-sulfanyl-3-phenylpropanoyl)Ala-Pro (*14*), compound **1**, or [(2*S*)-2-sulfanyl-3-phenylpropanoyl]Gly-(5-Ph)Pro, compound **2** (*15*), bind to NEP and TLN by a thiol-induced coordination of Zn²⁺ ion and by interacting with the S₁' and S₂' subsites of these enzymes (Table 1). This mode of enzyme recognition,

[‡] The atomic coordinates have been deposited at the Protein Data Bank, Brookhaven National Laboratory, Upton, NY: 1QF0 (compound **3**), 1QF1 (compound **4**), and 1QF2 (compound **2**).

* To whom correspondence should be addressed: Département de Pharmacochimie Moléculaire & Structurale, INSERM U266, CNRS UMR 8600, UFR des Sciences Pharmaceutiques & Biologiques, 4, avenue de l'Observatoire, 75270 Paris Cedex 06, France. Telephone: (33)-1-43.25.50.45. Fax: (33)-1-43.26.69.18. E-mail: roques@pharmacie.univ-paris5.fr.

[§] UFR des Sciences Pharmaceutiques et Biologiques.

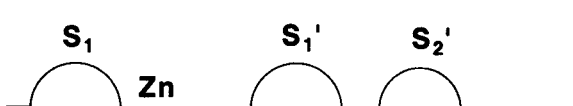
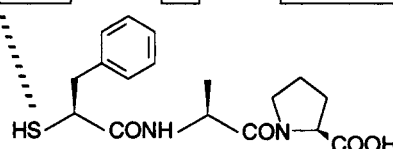
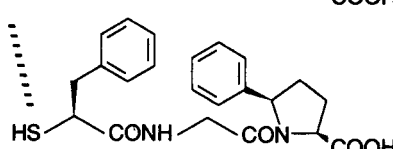
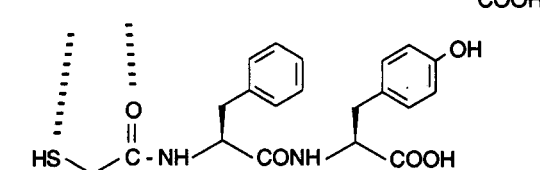
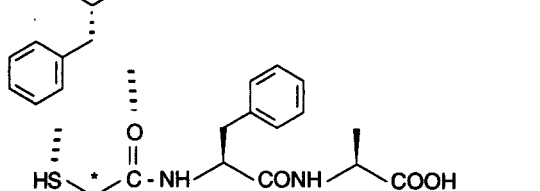
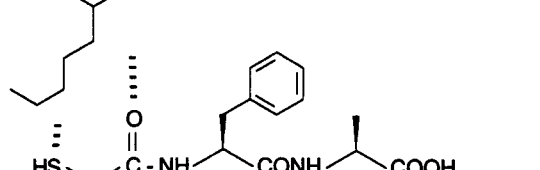
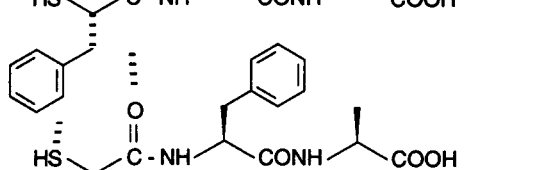
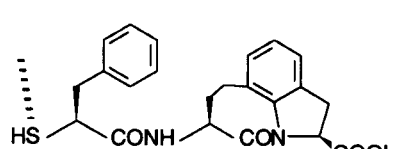
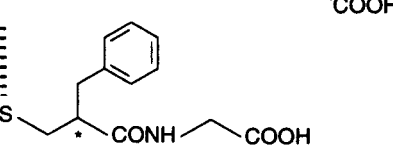
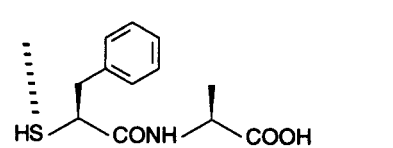
^{||} UFR des Sciences Pharmaceutiques et Biologiques.

[⊥] Present address: LURE, Bât. 209d, Université Paris Sud, 91405 Orsay Cedex, France.

¹ Abbreviations: thiorphan, *N*-(2-mercaptomethyl-3-phenylpropanoyl)-glycine; retro-thiorphan, 3-(1-mercaptomethyl-2-phenyl-1-aminopropyl)-3-oxopropanoic acid.

² The nomenclature used for the amino acid residues (P₁, P₁', P₂', ...) of an inhibitor and for the subsites (S₁, S₁', S₂', ...) of the enzyme is that of Schechter and Berger (*1*).

Table 1: Mode of Recognition of TLN by Various Mercaptoacyl Derivatives and Comparison of Their K_i Values on TLN, NEP, and ACE Activities^a

N°		TLN	NEP	ACE
		K_i (nM) ^b	K_i (nM) ^b	
1		200 ± 20	3.8 ± 0.6	0.3 ± 0.1
2 (RB 106)		1,200 ± 200	1.6 ± 0.3	0.55 ± 0.05
3		42 ± 1	2.9 ± 0.6	5.6 ± 0.6
4 ^b		48 ± 5	2.9 ± 0.5	n.d.
5		19 ± 4	2.3 ± 0.2	7.1 ± 0.5
6		1,000 ± 200	14 ± 2	220 ± 20
7 (CGS-28,106)		1,600 ^d	48 ^d	40 ^d
8 ^c (thiorphan)		1,600 ± 200	2.4 ± 0.8	70 ± 10
9		350 ± 10	4 ± 1	1,800 ± 200

^a The modes of binding of compounds 2–4 (this paper), 7 (16), and 8 (12) to TLN have been experimentally determined, and those of compounds 1, 5, 6, and 9 are inferred from their similarity to the related inhibitors cocrystallized with TLN (1 with 2, 5 and 6 with 4, and 9 with 2). ^b K_i values are the mean ± the standard error of the mean from three independent experiments performed in triplicate. ^c The asterisk indicates racemic asymmetric carbons. ^d From ref 16.

leaving the S_1 subsite empty, was also proposed to account for the binding of the tricyclic α -mercaptoacyl derivative CGS-28106 7 in TLN (16).

However, the spatial proximity of the thiol groups and the oxygen of the adjacent amide bond suggests that a zinc bidentation, previously demonstrated in the case of TLN for

inhibitors with hydroxamate (17) or carboxyl–zinc coordinating groups (11), could occur in the case of α -mercaptoacyldipeptides.

To investigate this possibility, three α -mercaptoacyldipeptides have been cocrystallized with TLN: [(2*S*)-2-sulfanyl-3-phenylpropanoyl]Gly-(5-Ph)Pro **2**, [(2*S*)-2-sulfanyl-3-phenylpropanoyl]Phe-Tyr **3**, and [(2*S,R*)-2-sulfanylheptanoyl]-Phe-Ala **4**.

A new mode of bidentate recognition of a metallopeptidase with a pentacoordination of the zinc ion and the occupancy of the S_1 , S_1' , and S_2' subsites was observed for compounds **3** and **4**. Conversely, as previously proposed (15), compound **2** acts as a monodentate for the zinc ion and occupies only the S_1' and S_2' subsites of TLN. This indicates that in this enzyme, the two types of binding modes are possible but are not equivalent in terms of stabilizing energies.

The comparison of the inhibitory potencies of the three compounds and various analogues of TLN, NEP, and ACE allows their proposed mode of binding to the two latter enzymes to be confirmed, and extends the way for designing new types of inhibitors.

EXPERIMENTAL PROCEDURES

Chemicals

[(2*S*)-2-Sulfanyl-3-phenylpropanoyl]Gly-(5-Ph)Pro (RB106) **2**, [(2*S*)-2-sulfanyl-3-phenylpropanoyl]Phe-Tyr **3**, and [(2*S,R*)-2-sulfanyl-heptanoyl]Phe-Ala **4** were synthesized in the laboratory as described previously (14, 15).

Biochemical Assays

Neutral endopeptidase from rabbit kidney (18) and angiotensin converting enzyme from rat testis (19) were purified to homogeneity as previously described. Thermolysin was from Sigma (France). Inhibitory potencies were determined by using [3 H]Tyr-Gly-Gly-Phe-Leu as the substrate for TLN ($K_m = 200 \mu\text{M}$) (20), *N*-Cbz-Phe-His-Leu ($K_m = 50 \text{ mM}$) as the substrate for ACE (21), and [3 H]Tyr-D-Ala²-Gly-Phe-Leu ($K_m = 30 \mu\text{M}$) as the substrate for NEP (22). Accounting for their competitive nature, the K_i values of the inhibitors were determined by using the Cheng–Prusoff relationship [$K_i = \text{IC}_{50}/(1 + [\text{S}]/K_m)$].

Crystallography

Crystallization. TLN was cocrystallized with the three different inhibitors using the hanging drop method, following the procedure described by Matthews et al. (23). For removal of added salts, 13 mg of lyophilized TLN was suspended in 0.7 mL of water and centrifuged at 7400g. The dottle was redissolved in 100 μL of solution A [50 mM tris(hydroxymethyl)aminomethane/acetate buffer (pH 8.0), 0.5 M $\text{Ca}(\text{CH}_3\text{COO})_2$, 4 mM dithiothreitol, 1 mM NaN_3 , and 45% (v/v) DMSO]. Enzyme concentrations were estimated using an ϵ_{280} of $56\,000 \text{ M}^{-1} \text{ cm}^{-1}$.

(1) **TLN Compound 2.** One microliter drops (110 mg/mL, 3.2 mM TLN, 17 mM **2** in solution A) were equilibrated against 1 mL of reservoir which contains 530 μL of solution A and 470 μL of water. Hexagonal crystals grew in 1 month at 5 °C.

Table 2: Statistical Data Recorded for the TLN–Inhibitor Complexes

	compound 2	compound 3	compound 4
space group	<i>P</i> 6 ₁ 22	<i>P</i> 6 ₁ 22	<i>P</i> 6 ₁ 22
parameters (Å)	<i>a</i> = <i>b</i> = 93.50 <i>c</i> = 131.30	<i>a</i> = <i>b</i> = 93.37 <i>c</i> = 131.79	<i>a</i> = <i>b</i> = 93.31 <i>c</i> = 131.83
crystal–plate distance (mm)	290	157	240
resolution (Å)	34.5–2.1	19.3–2.2	23.4–2.0
no. of unique reflections	21572	17923	23624
data redundancy	4.7	4.1	3.4
<i>R</i> _{sym} (%)	3.5	10.1	9.3
$\langle I/\sigma(I) \rangle$	13.1	7.3	8.0
overall completeness (%)	99.1	99.6	99.2

(2) **TLN Compound 3.** One microliter drops (115 mg/mL, 3.3 mM TLN, 30 mM **3** in solution A) were equilibrated against 1 mL of reservoir containing 420 μL of solution A and 580 mL of water. Hexagonal crystals grew in 2 weeks at 5 °C.

(3) **TLN Compound 4.** The crystals were obtained under nearly equivalent conditions with initial 1 μL drops (110 mg/mL) containing 3.2 mM TLN and 22 mM **4** in solution A, equilibrated against a mixture of 410 μL of solution A and 590 μL of water. Hexagonal crystals were obtained after about 2 weeks at 5 °C.

Data Collection. Diffraction data were recorded using the LURE synchrotron facility, in Orsay (France). TLN–**2**, TLN–**3**, and TLN–**4** crystal diffraction data were collected at wavelengths of 0.97 Å (**2** and **4**) and 1.01 Å (**3**) using 300 and 180 mm diameter MAR Research Image Plate systems, respectively, connected to the W32 and DW21b beam lines (24, 25). One single crystal of each TLN–inhibitor complex was used and roughly oriented with the crystallographic *c* axis at an angle of 20° to the rotation axis. With this orientation and for the hexagonal space group, a 40° total rotation is enough to collect a complete data set at 2.1, 2.2, and 2.0 Å resolution, respectively. Data were processed with the MOSFLM package (26), and then merged and scaled with SCALA and AGROVATA from the CCP4 suite (27). Table 2 summarizes the results of the processing.

Structure Refinement. The three structure refinements were carried out by following the same procedure. They started from the native TLN structure already refined at 1.6 Å resolution [PDB file name 1LNF (28)] (29). The thermal parameters were set to an overall $\langle B \rangle$ value deduced from Wilson plots ($\langle B \rangle = 15.5 \text{ Å}^2$ for **2**, $\langle B \rangle = 16.6 \text{ Å}^2$ for **3**, and $\langle B \rangle = 14.5 \text{ Å}^2$ for **4**). At the beginning of the refinements, the complexed dipeptide Val-Lys and all solvent molecules were removed from the model (29). Because the crystals of inhibitor–TLN complexes were isomorphous with respect to native TLN 1LNF, the refinements began with a rigid-body least-squares refinement [X-plor (30)], followed by refinement of the atomic positions by energy minimization at the initial resolution of 2.5 Å. This resolution was progressively increased to the maximum of 2.1 Å for **2**, 2.2 Å for **3**, and 2.0 Å for **4**. At this stage, grouped thermal parameters (two for each residue) were refined and around 50 water molecules located outside the active site were added in each structure. Using amplitudes where $F > 2\sigma(F)$, the residuals were as follows: for **2** ($d = 10\text{--}2.1 \text{ Å}$), $R_{\text{free}} = 27.8\%$ (31) and $R_{\text{fac}} = 23.2\%$; for **3** ($d = 10\text{--}2.2 \text{ Å}$), $R_{\text{free}} = 26.2\%$ and $R_{\text{fac}} = 21.4\%$; and for **4** ($d = 10\text{--}2.0 \text{ Å}$), $R_{\text{free}} =$

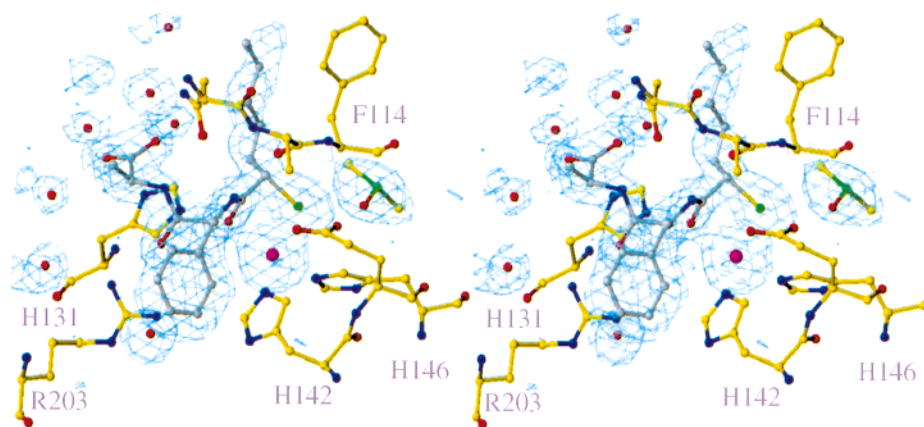


FIGURE 1: Stereodrawing showing a part of the active site region of TLN. The model (ball-and-stick), representing the fully refined structure, has been superimposed on difference electron density (contoured at 2σ) with coefficients ($F_o - F_c$, omit) based on the differences between observed amplitudes from the complex data set and calculated amplitudes from the refined model with the inhibitor and nearby solvent molecules removed. The map shows the *S* configuration of **4** at the level of C317, the atom bearing the thiol group. Thus, from the racemate of **4**, only one inhibitor has been selected by thermolysin during the diffusion process: magenta, Zn atom; gray, inhibitor; and yellow, enzyme side chains.

28.8% and $R_{\text{fac}} = 24.2\%$. In each structure, a Fourier difference map revealed a residual electron density located in the active site and corresponding to the complexed molecule. The thiol group was placed in the highest peak of the map near the Zn metal. The backbone and the substituents of the inhibitors were then constructed together in the well-shaped electron density. Files describing the inhibitors were created using X-plor parameters. Energy terms were empirically adjusted to those of X-plor. In the peculiar case of **4**, the absolute configuration of the thiol-substituted carbon remained unknown at this stage, and its pentyl substituent was not modeled. The following refinements consisted of a progressive introduction of solvent molecules with good geometry, and refinement of the individual thermal parameters and atomic positions. The quality of the refined models was regularly checked using Procheck (32), What-Check (33), and the RS-fit procedure of the O package (34). In the structure of **3**, after energy minimization, introduction of 50 water molecules and *B*-grouped refinements ($R_{\text{free}} = 25.2\%$, $R_{\text{fac}} = 21.0\%$), the configuration of the asymmetric carbon was unambiguously recognized as being only *S* form (Figure 1), and the aliphatic substituent was modeled.

In the three structures, the last Fourier difference maps exhibited two (**3** and **4**) or three (**2**) important residual densities which cannot be interpreted as water molecules because of the absence of putative H-bonding in a hydrophobic environment and because of a broad density shape. Although individual atomic positions cannot be distinguished, we best modeled these densities using DMSO molecules. One of them was previously observed in several structures of TLN [PDB file names 1HYT (35), 1LND (29), 1LNF (29), and 8TLN (36)]. In the very last step of refinement, the structures were refined against the whole set of crystallographic data, consequently without any R_{free} calculation. The statistics of the refined structures are summarized in Table 3.

RESULTS

The mercaptoacyldipeptides **2–4** have the general formula $\text{HS-CH(R}_1\text{)-CO-AA}_1\text{-AA}_2$. They mimic tripeptides $\text{H}_2\text{N-CH(R}_1\text{)-CO-AA}_1\text{-AA}_2$, with the N-terminal amino group re-

Table 3: Final Refinement Statistics for the TLN–Inhibitor Complexes

	TLN–2	TLN–3	TLN–4
resolution (Å)	10–2.1	10–2.2	10–2.0
final R_{fac} (%)	15.9	16.1	16.5
R_{free} (%) (before merging all the data)	22.2	21.6	22.4
no. of reflections used in refinement	21544	16963	22425
no. of degrees of freedom	11220	10584	10700
no. of water molecules	235	167	204
no. of DMSO molecules	3	2	2
estimated error on coordinates (Sigmaa) (%)	0.16	0.16	0.16
rmsd for bond lengths (Å)	0.008	0.008	0.008
rmsd for bond angles (deg)	1.38	1.38	1.38
rmsd for dihedral angles (deg)	23.6	23.7	23.6
rmsd for improper angles (deg)	1.15	1.15	1.15
overall $\langle B \rangle$ (Å ²)	13.1	10.8	12.1
protein $\langle B \rangle$ (Å ²)	10.9	9.7	10.8
solvent $\langle B \rangle$ (Å ²)	32.1	24.0	27.3
inhibitor $\langle B \rangle$ (Å ²)	27.0	14.2	11.0

placed with a thiol. Consequently, the various atoms of these three residues are numbered 317 for the sulfanyl moiety $\text{HS-CH(R}_1\text{)-CO}$ and 318 and 319 for amino acids AA_1 and AA_2 , respectively.

The refined models of complexes exhibited two different binding modes for the inhibitors of TLN (Figure 2). The interaction of **2** with TLN was identical to that previously proposed from molecular modeling (15), whereas a new binding mode was observed for TLN–**3** and TLN–**4**, which, to the best of our knowledge, was not described yet for zinc metalloproteases.

Metal Binding. The inhibitors **3** and **4** interact through bidentate with the zinc atom, the sulfur and the oxygen of the mercaptoacyl function being coordinated to the metal with distances of 2.3 and 2.4 Å, respectively. The five zinc ligands form a distorted trigonal bipyramid. NE2 (His¹⁴⁶) and the carbonyl oxygen of the inhibitor occupy axial positions, while the sulfur ligand S (317) and the coordinating enzyme amino acids, NE2 (His¹⁴²) and OE2 (Glu¹⁶⁶), are in a planar position. In such a conformation, the O (317), liganded to zinc, is also close to NE2 (His²³¹) and the sulfur atom is 3.1 Å from the OE1 of Glu¹⁴³ (Figure 2b,c).

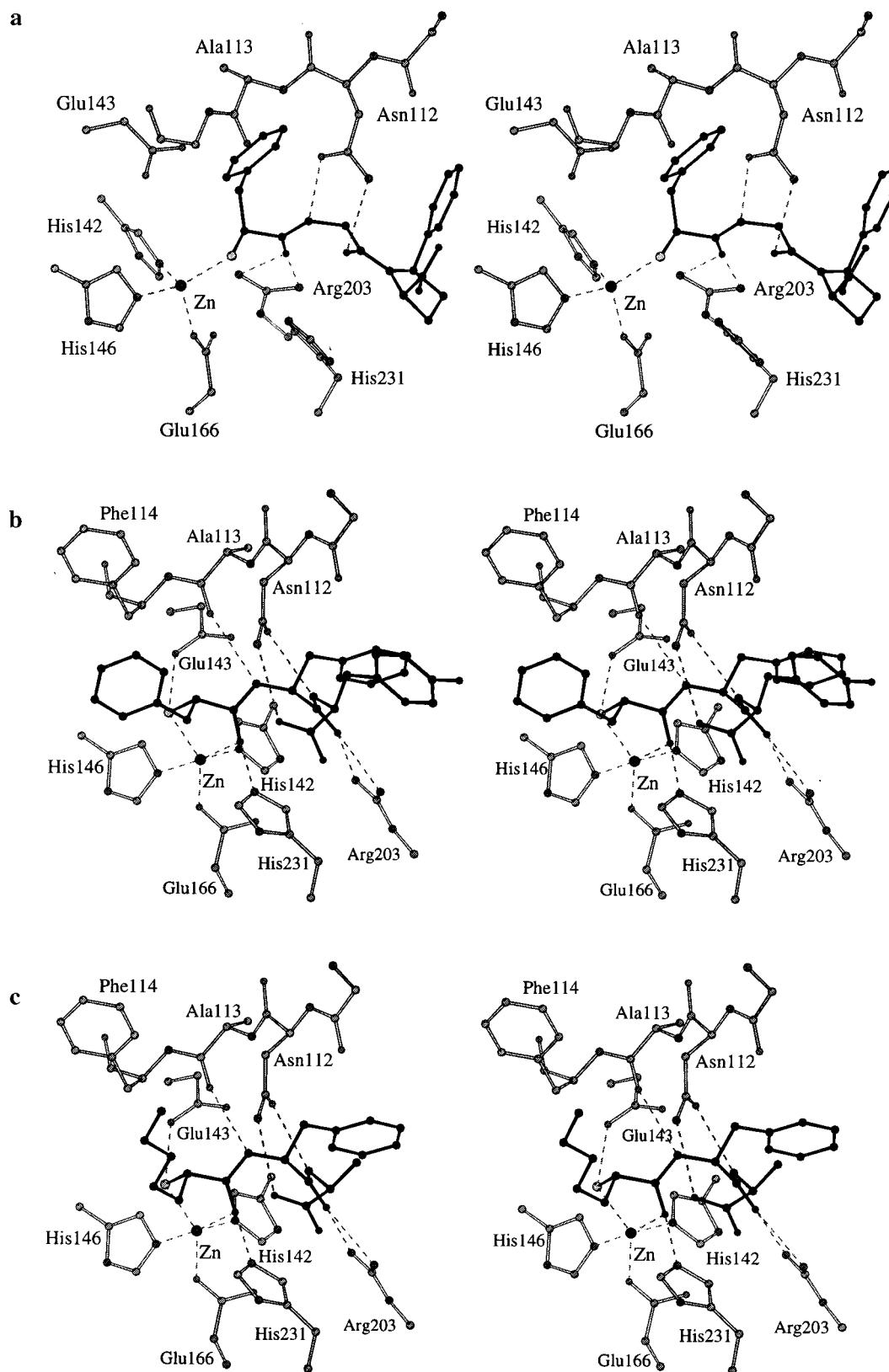


FIGURE 2: Refined structures of inhibitors **2** (a), **3** (b), and **4** (c) in the active site of thermolysin. Presumed hydrogen bonds and interactions with the Zn ion are drawn as dashed lines.

The Zn coordination in the TLN-2 complex is approximately tetrahedral with three ligands provided by TLN [NE2 (His¹⁴⁶), NE2 (His¹⁴²), and OE2 (Glu¹⁶⁶)] and the fourth provided by the sulfur atom of the mercapto inhibitor (Figure 2a).

H-Bonding of the Inhibitor Backbones in the Active Site. In the crystal structures of TLN-3 and TLN-4, the backbone conformations are similar to those modeled for the natural substrate in the transition state (3) (Figure 2b,c). Thus, the zinc atom is pentacoordinated with a binding mode

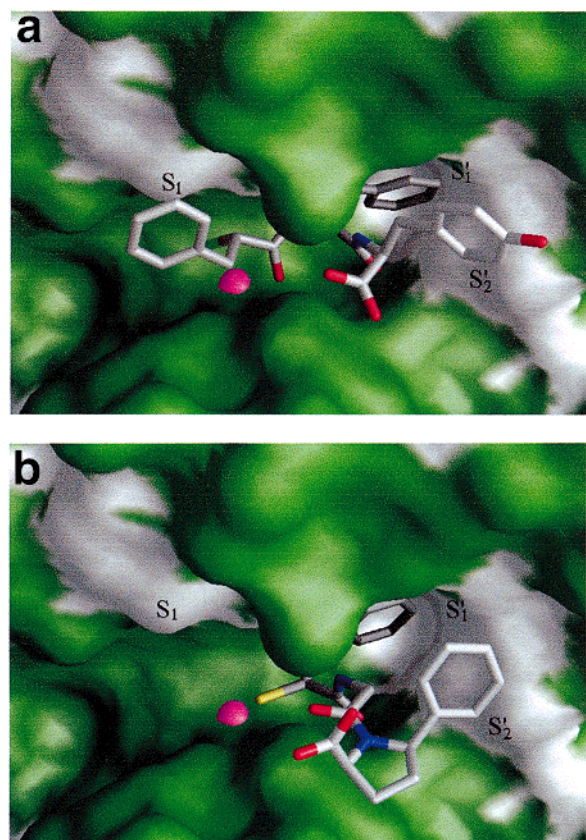


FIGURE 3: Inhibitors **3** (a) and **2** (b) are represented on the molecular surface of the active site of thermolysin. The orientation is the same as in Figure 2. The code of colors for the TLN surface is as follows: gray, hydrophobic residues; violet, Zn atom; and green, hydrophilic residues and backbone.

which implies that O (317) and S (317) take the place of the oxygen atom of the cleavable peptide bond of the substrate and that of the catalytic water molecule, respectively. Moreover, they exhibit equivalent H-bonding in the active site; the NH of the P₁' component (Phe³¹⁸) is connected to the CO of Ala¹¹³, and the CO of Phe³¹⁸ is doubly bonded to the guanidinium group of Arg²⁰³. The CONH₂ group of Asn¹¹² functions as both a hydrogen bond acceptor and donor group toward the HN and C-terminal carboxyl groups of the P₂' amino acid (Tyr³¹⁹ in **3** and Ala in **4**), respectively. The terminal carboxyl group was also found to be bound with three water molecules. This hydration network is observed in the two structures.

In the case of the TLN–**2** complex (Figure 2a), the backbone of the inhibitor is shifted by one amino acid toward the S' subsites compared to those of the TLN–**3** and TLN–**4** complexes, leaving the S₁ subsite empty. The O (317) atom forms a double hydrogen bond with the guanidinium group of Arg²⁰³, and the N and O atoms of Phe³¹⁸ are connected to OD1 and ND2 of Asn¹¹², respectively. The proline residue did not interact with TLN and is located outside the active site with hydrogen bonds formed between its carboxyl group and water molecules.

Subsite Binding. For inhibitors **3** and **4**, the substituent R₁ and the side chains of AA₁ and AA₂ bind subsites S₁, S₁', and S₂', respectively. As shown in Figure 3a, the S₁ and S₂' subsites form pockets with partially lipophilic surfaces, whereas S₁' is a deep hydrophobic cavity. In both structures, AA₁ is a Phe residue (P₁' component) which fits well in the

S₁' subsite. Its very low thermal parameters (6.7 Å² for **3** and 8.5 Å² for **4**) are reminiscent of tight binding.

The R₁ substituent of **3** is a benzyl group whose aromatic ring is oriented toward the side chains of Asn¹¹², Phe¹¹⁴, and Tyr¹⁵⁷. Nevertheless, no stacking effect was observed. The same contacts are observed with these residues in the TLN–**4** structure, where the R₁ substituent of the inhibitor is a pentyl chain. In agreement with the increased degrees of freedom of R₁, the corresponding thermal parameters (for R₁–**3**, $\langle B \rangle = 11.0$ Å², and for R₁–**4**, $\langle B \rangle = 21.9$ Å²) are higher than those observed for the P₁' component. In both structures, R₁ is also found in hydrophobic contact with one DMSO molecule located at the end of the S₁ binding site, but this interaction did not significantly mask R₁ from the solvent.

Further interactions of both inhibitors with TLN differ at the level of the S₂' subsite. In **4**, the side chain of AA₂ (Ala) points toward the S₂' subsite with van der Waals contact with Leu²⁰². In the TLN–**3** structure, the corresponding side chain is a tyrosine, whose phenyl group completely fills the S₂' subsite cavity. However, interactions are not very well optimized in this region as shown by the relatively high *B*-factor of the Tyr side chain ($\langle B \rangle = 28.1$ Å²) compared to those of other substituents located in S₁ or S₁' subsites. No hydrogen bond was observed for the phenol group.

Compound **2** (RB106) exhibits a different mode of binding, which is similar to that proposed for the CGS-28106 inhibitor (**16**) (Figure 3b). The benzyl of R₁ occupies the S₁' subsite. Compared to the position of the phenyl ring of **3** and **4** in the same subsite, a shift of 1.3 Å is observed. Moreover, the thermal parameters are relatively high ($\langle B \rangle = 21.2$ Å²). The phenyl ring of the phenyl proline AA₂ fits the S₂' subsite of the enzyme as this occurs with Tyr in the TLN–**3** complex (Figure 3b), and the proline is outside the active site.

Inhibitory Potencies of Various Mercaptoacyl Derivatives toward TLN, NEP, and ACE. The inhibitory potencies of various α - and β -mercaptoacyldipeptides were reported in Table 1 for the three enzymes. For TLN, these compounds could be classified in two categories. The first series contains compounds **1**, **2**, and **6–9**, which have *K_i* values in the 10^{–6} M range. The second series contains compounds **3–5**, which have inhibitory potencies in the 10^{–8} M range. The large difference in the *K_i* values between the two series of compounds could be related to a different mode of binding to TLN. For NEP inhibition, all the compounds have *K_i* values in the nanomolar range which could reflect an identical mode of recognition of the active site of this peptidase. A slight decrease in potency was observed for **6** and **7** which have *K_i* values in the 10^{–8} M range. For ACE inhibition, α -mercaptoacyldipeptides **1–5** have *K_i* values in the nanomolar (**3** and **5**) or sub-nanomolar (**1** and **2**) range, indicating a full occupancy of the active site, as compared to compounds **6**, **8**, and **9** which have *K_i* values between 10^{–6} and 10^{–8} M.

DISCUSSION

Several sulfhydryl-containing inhibitors have been cocrystallized with TLN for the purpose of investigating their binding mode and ultimately developing hypotheses for their interactions with the active sites of related zinc metallopeptidases such as ACE and NEP. The compounds used

Table 4: Zinc Coordination in the Inhibitor–Thermolysin Complexes

	compound 2	compound 3	compound 4
angles (deg)			
NE2 (His ¹⁴⁶)–Zn–O (317)	–	172.2	172.3
NE2 (His ¹⁴⁶)–Zn–S (317)	126.1	96.7	95.6
NE2 (His ¹⁴⁶)–Zn–NE2 (His ¹⁴²)	107.2	95.0	92.3
NE2 (His ¹⁴⁶)–Zn–OE2 (Glu ¹⁶⁶)	89.4	91.7	90.2
NE2 (His ¹⁴²)–Zn–S (317)	109.5	120.5	119.9
NE2 (His ¹⁴²)–Zn–OE2 (Glu ¹⁶⁶)	121.1	117.9	114.3
distances (Å)			
NE2 (His ¹⁴⁶)–Zn	2.1	2.2	2.2
O (317)–Zn	–	2.4	2.4
S (317)–Zn	2.3	2.4	2.3
NE2 (His ¹⁴²)–Zn	2.0	2.1	2.1
OE2 (Glu ¹⁶⁶)–Zn	1.9	2.0	2.0

previously belonged to β -thiol inhibitors such as (2-benzyl-3-mercaptopropionyl)-L-alanine glycine amide (BAG) (37), thiorphan¹ and retrothiorphan (12), or an α -thiol inhibitor such as CGS-28106 (16) (Table 1). All these compounds are rather poor inhibitors of TLN, with K_i values in the 10^{-6} M range, and behave as monodentate inhibitors with a roughly tetrahedral coordination of the zinc atom as observed for **2** in this study (Table 1 and Figure 2a). In this binding mode, the sulfur atom is located 1.9–2.4 Å from the Zn, probably in a deprotonated form. Moreover, diffraction studies have shown that the S_1' subsite is fitted by the benzyl groups of these inhibitors and the S_2' subsite by hydrophobic residues, the S_1 subsite remaining empty.

In this study, we show for the first time that mercaptoacyldipeptides, with K_i values in the 10^{-8} M range, such as compounds **3** and **4**, interact with the S_1 subsite of TLN. In this case, the pentacoordination of the Zn atom corresponds to a trigonal bipyramid, and the side chains of AA₁ and AA₂ now interact with subsites S_1' and S_2' (Table 1) (Figure 2b,c). These observations could account for the high affinity of these mercaptoacyldipeptides for TLN.

With this aim, two kinds of interactions have to be taken into account: (i) the binding of the inhibitor with the Zn atom and neighboring residues and (ii) the interactions of the inhibitor side chains with S_1 , S_1' , and S_2' subsites.

Zn Coordination Sphere. Compared to a tetrahedral geometry, the pentacoordination of Zn found in **3** and **4** implies new electrostatic interactions in the vicinity of the zinc atom (Figure 2b,c and Table 4).

In previous crystal structures of TLN cocrystallized with mercapto inhibitors and characterized by a Zn^{2+} tetracoordination, the thiol group, located at 1.9–2.4 Å from the metal ion, was proposed to be deprotonated (at pH 8) because the Zn^{2+} ion is expected to act as a Lewis acid by lowering the pK_a value of the SH group. However, in the structures presented here (compounds **3** and **4**), the OE1 of Glu¹⁴³ is located 3.1 Å from the sulfur atom. The distance is too small to consider the possibility that both the sulfhydryl and carboxylate functions are negatively charged. Furthermore, the OE1...S–C α angle of 116° and the CD–OE1...S angle of 128° suggest that OE1 and S are H-bonded and consequently that at least one of these atoms is protonated.

The second ligand of the zinc atom is the oxygen of the mercaptoacyl function in inhibitors **3** and **4**. It is located 2.4 Å from Zn^{2+} in both structures. However, this atom is also

2.7 Å from NE2 of His²³¹, suggesting the occurrence of a strong electrostatic interaction with the protonated imidazole group. This is in accordance with results of mutagenesis experiments performed on the TLN-like protease produced by *Bacillus stearothermophilus*. Thus, the replacement of His²³¹, with Phe or Ala, was shown to drastically reduce the affinity of the mutated enzyme for hydroxamate, carboxylate, or phosphonic inhibitors (38). Conversely, the weak effect on the K_i values of **4** toward H231F and H231A mutants suggests that, in this case, the loss of the electrostatic interaction between NE2 of His²³¹⁺ and the negatively charged oxygen of the mercaptoacyl carbonyl group is probably offset by an enhancement of the interaction between this oxygen and the Zn ion in both mutants.

Finally, the NH of the mercaptoamide function is hydrogen bonded to the carbonyl of Ala¹¹³. All these interactions have been previously found in the complexes of TLN and bidentate inhibitors bearing a carboxylate (CLT), phosphonate (ZG^PLL or ZF^PLA), and hydroxamate as zinc-coordinating moieties (2). They have been proposed to mimic the interactions occurring between the substrate and the enzyme during the hydrolysis of the peptide bond. It can be observed that the mercaptoacyl moiety creates the same stabilizing network of H bonds as that occurring in the transition state.

Contributions of the Different Inhibitor Side Chains to TLN Subsite Binding. Compounds **3** and **4** have very similar conformations (rmsd = 0.26 Å) and identical modes of binding to TLN. Their K_i values for TLN are 42 nM for (S)-**3** and 48 nM for (R,S)-**4**. However, as our work shows unambiguously that only the S enantiomer of **4** was found cocrystallized with TLN, we could assume that the K_i value of the optically pure (S)-**4** is lower. The importance of the S_1 recognition is clearly demonstrated by the 50-fold lower inhibitory potency of **6**, a compound differing from **4** and **5** only by the removal of the aliphatic or aromatic side chain shown in **4** to fit the S_1 subsite. It can be assumed that **6** interacts like **4** and **5** by a zinc bidentation. Indeed, a single interaction with Zn by the SH group would have shifted the inhibitor inside the TLN active site, resulting in an empty S_1' subsite (Table 1). Therefore, the lower K_i of **6** is mainly due to the loss of hydrophobic interactions occurring between the R₁ side chain and the S_1 subsite, and probably also to the higher flexibility of the mercaptoacetyl group.

In compound **3**, the *p*-hydroxyphenyl group located in the S_2' subsite of TLN did not improve the TLN recognition as shown by the fact that the K_i value was lower for **3** than for **5**. This is in agreement with the experimental observation that the phenol group has relatively high thermal parameters, due to the large degree of accessibility of the S_2' subsite at the surface of the enzyme, in the TLN–**3** structure. This has been previously observed in the TLN–CLT structure (11) in which the tryptophan residue of the inhibitor, located in the P_{2'} position, also has high thermal parameters.

The difference in the binding mode of compounds **1**, **2**, and **7–9** versus that of **3–5** in TLN accounts for their K_i values; the bidentation of Zn^{2+} ion and the occupancy of the S_1 subsite induce a 2 order of magnitude increase in affinity compared to those of inhibitors which interact only with the S_1' and S_2' subsites and act as Zn monodentates. The different modes of binding of the α -mercaptoacyl inhibitors to TLN are easily explained by the size of the S_2' subsite which cannot accommodate bulky groups such as

proline (compound **1**), substituted prolines (compound **2**), or tricyclic structure (compound **7**).

If we analyze the affinities of the different inhibitors for the TLN-related enzymes, ACE and NEP, large differences are observed. Thus, in the case of ACE, all the α -mercaptoacyl dipeptides, except **6**, have nanomolar or sub-nanomolar K_i values. Due to the well-known ability of the S_1 subsite to accept hydrophobic linear or aromatic side chains, the interaction with ACE is optimized with these molecules interacting very likely with the S_1 , S_1' , and S_2' subsites and acting as zinc bidentates. As in the case of TLN, the substitution of $R_1 = \text{CH}_2\text{-Ph}$ in **5** with H (compound **6**) decreases the affinity for ACE by a factor 30, illustrating the existence of hydrophobic interactions in the S_1 subsite.

In contrast with TLN and ACE, no significant variations in K_i values for the inhibitors were observed for NEP. Thus, all the α -mercaptoacyl dipeptides **1–5** have K_i values in the nanomolar range, as do thiorphan **8** and compound **9**, which recognize only the S_1' and S_2' subsites, suggesting that their mode of binding to the peptidase is similar, as previously proposed (14). It is well-known that the S_2' subsite of NEP, as well as that of TLN, does not recognize proline derivatives or bulky cyclic structures (39), meaning that the C-terminal residues of **1**, **2**, and **7** are located outside the active site.

This shows the minor stabilizing role of the putative S_1 subsite in NEP already underlined with compounds such as phosphinic-containing inhibitors $R_1\text{-P(O)OH-CH}_2\text{CH(R}_1'\text{)-CONH(R}_2'\text{)COOH}$ (40), which exhibit only a slightly increased affinity for NEP compared to that of thiorphan despite the topologically imposed presence of a P_1 side chain. This could suggest that the S_1 subsite of NEP is probably different and/or less accessible than that of TLN or ACE.

In conclusion, a new mode of thermolysin recognition has been characterized in this work with a bidentation of the zinc atom by both a thiol and an oxygen group, opening the way for the design of new types of inhibitors.

ACKNOWLEDGMENT

We gratefully acknowledge E. Ruffet for enzymatic experiments and C. Dupuis for expert drafting of the manuscript.

REFERENCES

- Schechter, I., and Berger, A. (1967) *Biochem. Biophys. Res. Commun.* **27**, 157–162.
- Matthews, B. W. (1988) *Acc. Chem. Res.* **21**, 333–340.
- Hangauer, D. G., Monzingo, A. F., and Matthews, B. W. (1984) *Biochemistry* **23**, 5730–5741.
- Roques, B. P., Noble, F., Dauge, V., Fournié-Zaluski, M. C., and Beaumont, A. (1993) *Pharmacol. Rev.* **45**, 87–145.
- Wyvratt, M. J., and Patchett, A. A. (1985) *Med. Res. Rev.* **5**, 483–531.
- Cheng, X. M., Ahn, K., and Haleen, S. J. (1997) Cardiovascular and Pulmonary Diseases, *Ann. Rep. Med. Chem.* **32**, 61–70.
- Roques, B. P. (1993) *Biochem. Soc. Trans.* **21**, 678–685.
- Marie-Claire, C., Ruffet, E., Antonczak, S., Beaumont, A., O'Donohue, M., Roques, B. P., and Fournié-Zaluski, M. C. (1997) *Biochemistry* **36**, 13938–13945.
- Marie-Claire, C., Ruffet, E., Tiraboschi, G., and Fournié-Zaluski, M. C. (1998) *FEBS Lett.* **438**, 215–219.
- Tiraboschi, G., Jullian, N., Thery, V., Antonczak, S., Fournié-Zaluski, M. C., and Roques, B. P. (1999) *Protein Eng.* **12** (2), 141–149.
- Monzingo, A. F., and Matthews, B. W. (1984) *Biochemistry* **23**, 5724–5729.
- Roderick, S. L., Fournié-Zaluski, M. C., Roques, B. P., and Matthews, B. W. (1989) *Biochemistry* **28**, 1493–1497.
- Ksander, G. M., de Jesus, R., Yuan, A., Ghai, R. D., Trapani, A., McMartin, C., and Bohacek, R. (1997) *J. Med. Chem.* **40**, 495–505.
- Coric, P., Turcaud, S., Meudal, H., Roques, B. P., and Fournié-Zaluski, M. C. (1996) *J. Med. Chem.* **39**, 1210–1219.
- Fournié-Zaluski, M. C., Coric, P., Thery, V., Gonzalez, W., Meudal, H., Turcaud, S., Michel, J. B., and Roques, B. P. (1996) *J. Med. Chem.* **39**, 2594–2608.
- Bohacek, R., De Lombaert, S., McMartin, C., Priestle, J., and Grüter, M. (1996) *J. Am. Chem. Soc.* **118**, 8231–8249.
- Holmes, M. A., and Matthews, B. W. (1981) *Biochemistry* **20**, 6912–6920.
- Aubry, M., Berteloot, A., Beaumont, A., Roques, B. P., and Crine, P. (1987) *Biochem. Cell Biol.* **65**, 398–404.
- Pantoliano, M. W., Holmquist, B., and Riordan, J. F. (1984) *Biochemistry* **23**, 1037–1042.
- Benchetrit, T., Fournié-Zaluski, M. C., and Roques, B. P. (1987) *Biochem. Biophys. Res. Commun.* **147**, 1034–1040.
- Piquilloud, Y., Reinharz, A., and Roth, M. (1970) *Biochim. Biophys. Acta* **206**, 136–142.
- Llorens, C., Malfroy, B., Schwartz, J. C., Gacel, G., Roques, B. P., Roy, J., Morgat, J. L., and Javoy-Agid, F. A. (1982) *J. Neurochem.* **39**, 1081–1089.
- Matthews, B. W., Jansonius, J. N., Colman, P. M., Shoenborn, B., and Dupourque, D. (1972) *Nat. New Biol.* **238**, 37–41.
- Fourme, R., Dhez, P., Benoit, J. P., Kahn, R., Dubuisson, J. M., Besson, P., and Frouin, J. (1992) *Rev. Sci. Instrum.* **63**, 982–987.
- Ramin, M., Shepard, W., Fourme, R., and Kahn, R. (1999) *Acta Crystallogr. D* **55**, 157–167.
- Leslie, A. G. W. (1990) *Crystallogr. Comput.* **5**, 50–61.
- Collaborative Computational Project, Number 4 (1994) *Acta Crystallogr. D* **50**, 760–764.
- Bernstein, F. C., Koetzle, T. F., Williams, G. J., Meyer, E. E., Brice, M. D., Rodgers, J. R., Kennard, O., Shimanouchi, T., and Tasumi, M. (1977) *J. Mol. Biol.* **112**, 535–542.
- Holland, D. R., Hansrath, A. C., Juers, D., and Matthews, B. W. (1995) *Protein Sci.* **4**, 1955–1965.
- Brünger, A. T., Krukowski, A., and Erickson, J. W. (1990) *Acta Crystallogr. A* **46**, 585–593.
- Brünger, A. T. (1992) *Nature* **355**, 472–475.
- Laskowski, R. A., MacArthur, M. W., Moss, D. S., and Thornton, J. M. (1993) *J. Appl. Crystallogr.* **26**, 283–291.
- Hooft, R. W., Vriend, G., Sander, C., and Abola, E. E. (1996) *Nature* **381**, 272.
- Jones, T. A., Zou, J. Y., Cowan, S. W., and Kjeldgaard, M. (1991) *Acta Crystallogr. A* **47**, 110–119.
- Hausrath, A. C., and Matthews, B. W. (1994) *J. Biol. Chem.* **269**, 18839–18842.
- Holland, D. R., Tronrud, D. E., Pley, H. W., Flaherty, K. M., Stark, W., Jansonius, J. N., McKay, D. B., and Matthews, B. W. (1992) *Biochemistry* **31**, 11310–11316.
- Monzingo, A. F., and Matthews, B. W. (1982) *Biochemistry* **21**, 3390–3394.
- Beaumont, A., O'Donohue, M. J., Paredes, N., Rousselet, N., Assicot, M., Bohuon, C., Fournié-Zaluski, M. C., and Roques, B. P. (1995) *J. Biol. Chem.* **270**, 16803–16808.
- Fournié-Zaluski, M. C., Lucas, E., Waksman, G., and Roques, B. P. (1984) *Eur. J. Biochem.* **139**, 267–274.
- Chen, H., Noble, F., Coric, P., Fournié-Zaluski, M. C., and Roques, B. P. (1998) *Proc. Natl. Acad. Sci. U.S.A.* **95**, 12028–12033.
- Ksander, G. M., de Jesus, R., Yuan, A., Ghai, R. D., Trapani, A., McMartin, C., and Bohacek, R. (1997) *J. Med. Chem.* **40**, 506–514.

BI991043Z